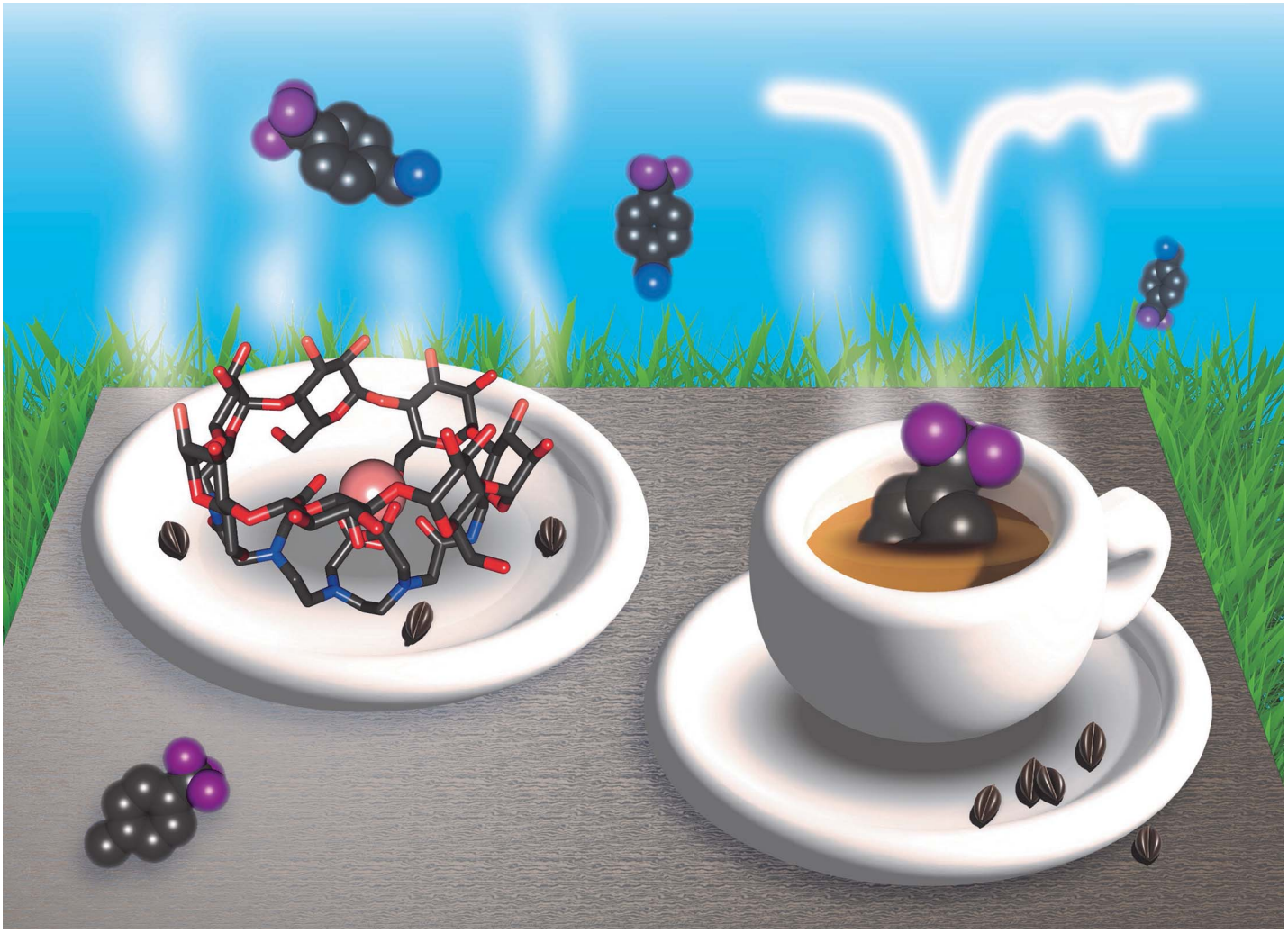

Showcasing research from Professor Amnon Bar-Shi's laboratory, Department of Molecular Chemistry and Materials Science, Weizmann Institute of Science, Rehovot, Israel.

NMR exchange dynamics studies of metal-capped cyclodextrins reveal multiple populations of host–guest complexes in solution

The guest exchange saturation transfer GEST NMR method was used to study exchange dynamics in systems composed of Ln-α-CDs or Ln-β-CDs with different guests, revealing multiple co-existing populations of host-guest complexes exclusively in solutions containing Ln-β-CDs. The enhanced spectral resolution of paramagnetic GEST (paraGEST), achieved by a strong pseudo contact shift induction of lanthanides, revealed that molecular guests could adopt multiple orientations within Ln-β-CDs' cavities, and in contrast, only a single orientation inside Ln-α-CDs. We concluded that paraGEST is a convenient tool for studying additional supramolecular systems of metal-capped molecular hosts.

As featured in:

See Amnon Bar-Shir *et al.*, *Chem. Sci.*, 2023, **14**, 11351.

ROYAL SOCIETY OF CHEMISTRY

rsc.li/chemical-science

Registered charity number: 207890

Chemical Science

ROYAL SOCIETY OF CHEMISTRY

EDGE ARTICLE

View Article Online
View Journal | View Issue

Cite this: *Chem. Sci.*, 2023, **14**, 11351

All publication charges for this article have been paid for by the Royal Society of Chemistry

NMR exchange dynamics studies of metal-capped cyclodextrins reveal multiple populations of host–guest complexes in solution†

Elad Goren, [a] Mark A. Iron, [b] Yael Diskin-Posner, [b] Alla Falkovich,[b] Liat Avram [b] and Amnon Bar-Shir *[a]

Metal-capped molecular hosts are unique in supramolecular chemistry, benefitting from the inner cavity's hydrophobic nature and the metal center's electrochemical properties. It is shown here that the paramagnetic properties of the metals in lanthanide-capped cyclodextrins (Ln-α-CDs and Ln-β-CDs) are a convenient NMR indicator for different populations of host–guest complexes in a given solution. The paramagnetic guest exchange saturation transfer (paraGEST) method was used to study the exchange dynamics in systems composed of Ln-α-CDs or Ln-β-CDs with fluorinated guests, revealing multiple co-existing populations of host-guest complexes exclusively in solutions containing Ln-β-CDs. The enhanced spectral resolution of paraGEST, achieved by a strong pseudo contact shift induction, revealed that different molecular guests can adopt multiple orientations within Ln-β-CDs' cavities and, in contrast, only a single orientation inside Ln-α-CDs. Thus, paraGEST, which can significantly improve NMR detectability and spectral resolution of host-guest systems that experience fast exchange dynamics, is a convenient tool for studying supramolecular systems of metal-capped molecular hosts.

Received 14th July 2023
Accepted 4th September 2023

DOI: 10.1039/d3sc03630h

rsc.li/chemical-science

Introduction

Cyclodextrins (CDs) are remarkable among the water-soluble molecular hosts used in host–guest supramolecular systems.[1–4] These highly water-soluble cyclic oligosaccharides have a hydrophobic cavity that allows them to form complexes with various guests, ranging from small organic molecules to proteins.[5–7] The industrial-scale production of CDs, the range of cavity sizes, and their straightforward chemical modifications make CD–guest complexes attractive in many fields of science and technology. These hosts are used to overcome the poor water solubility of drugs and improve their stability in bio-fluids.[8] In addition, they are used in electrochemical[9] and optical sensing[10] for capturing volatile analytes,[11] and as the immobilized phase in liquid chromatography.[12] CDs are utilized as building blocks in supramolecular polymers,[13] molecular switches,[14] and self-healing materials,[15] and as reaction catalysts.[16,17] Furthermore, coupling their catalytic abilities with their inherent chirality makes them attractive as enzyme mimetics.[5,18] Attaching a metal center to CDs, to obtain metallo-CDs,[19] evolved a whole new family of artificial metallo-enzymes, where the metal center plays a main role in both substrate binding and catalysis.[20]

The metal center in metallo-CDs can be bound to the CD rim either by a flexible linker or a rigid bridge, with the latter forming capped metallo-CDs,[21] in analogy to other metallo-cavitands.[22] The features of the metal element in capped metallo-CDs and the proximity between a cavity-bound ligand (*i.e.*, the guest) and the metal result in improved catalytic activities,[23–27] and is also used for other applications.[28–30] While metallo-CDs have been extensively studied, several factors can make their characterization in solutions challenging using traditional methods. For one, metallo-CDs host–guest systems are often dynamic, with a fast equilibrium between the hosted and free guest states. In addition, guest molecules may have multiple orientations inside the host's cavity,[31–33] creating different carceroisomers,[34,35] or they may bind the host in various host : guest stoichiometries[36] that complicate the analysis of titration data.[37] Furthermore, it was demonstrated that metallo-CD host could deform from its native CD shape or may have the metal center in different positions relative to the CD cavity.[38,39] Consequently, novel and advanced methods for studying such dynamic systems are needed.

NMR is frequently used to study and characterize host–guest systems in solutions,[32] but commonly used NMR techniques cannot handle systems involving fast exchange dynamics, low binding affinities, or short relaxation times – all of which are expected for metallo-CDs. The chemical exchange saturation transfer (CEST) method, developed for MRI studies,[40,41] has been

[a]*Department of Molecular Chemistry and Materials Science, Weizmann Institute of Science, Rehovot 7610001, Israel. E-mail: amnon.barshir@weizmann.ac.il*

[b]*Department of Chemical Research Support, Weizmann Institute of Science, Rehovot 7610001, Israel*

† Electronic supplementary information (ESI) available. See DOI: https://doi.org/10.1039/d3sc03630h

transformed to study host–guest complexes with fast dynamic interactions in supramolecular systems. In such cases, the method is called guest exchange saturation transfer (GEST).[42] This NMR-based approach takes advantage of the reversible, relatively fast, noncovalent interactions to: (i) identify "invisible" complexed guests in the NMR spectra, (ii) quantify exchange rates, and (iii) evaluate energy barriers.[43] Using a fluorinated guest, the background-free ^{19}F-GEST method has been recently used in the study of a variety of molecular hosts, such as cucurbit[*n*]urils,[44] bambus[*n*]urils,[45] deep-cavity cavitands,[46] pillar[*n*]arenes,[47] and supramolecular cages.[48]

Recently, ^{19}F-GEST was extended to ^{19}F-paraGEST (paramagnetic ^{19}F-GEST) to study paramagnetic molecular hosts.[30] In paraGEST, the resolution of the GEST spectrum (or z-spectrum) can be enhanced by increasing the chemical shift offset ($\Delta\omega$) between the NMR resonances of free and bound guest molecules, which is caused by the pseudo contact shift (PCS) induction capabilities of the paramagnetic element in the host. The requirement to obtain a GEST effect is that $\Delta\omega > k_{ex}$ (where k_{ex} is the exchange rate between bound and free guest states, and $\Delta\omega$ is defined in Hz units). Thus, the guest's proximity to a paramagnetic specie and the PCS induction capability of the metal increase $\Delta\omega$ and, consequently, the range of detectable exchange rates. As such, paraGEST is a powerful tool to study supramolecular systems that experience fast exchange dynamics, including metallo-cavitands, and can potentially uncover host–guest interactions that other analytical tools cannot capture. Herein, we use ^{19}F-paraGEST NMR to study host–guest systems of paramagnetic metallo-CDs, specifically lanthanide-capped cyclodextrins (Ln-α-CDs and Ln-β-CDs). This allowed us to identify at least two distinctive, coexisting 1 : 1 Ln-β-CD : guest populations in solution, having similar thermodynamic and kinetic properties. In contrast, only a single host–guest population was observed for the smaller and more symmetric Ln-α-CDs, even when using the largest possible PCS induction property. Our findings shed a light on the very different binding features of organic molecules to metal-caped α- and β-CDs in water.

Results and discussion

A family of metallo-β-CDs was synthesized[28] from the corresponding 6^A,6^D-diamino-6^A,6^D-dideoxy-β-cyclodextrin (diamino-β-CD, Fig. S1–S9†), in correlation to the family of metallo-α-CDs previously synthesized and described by us (Fig. 1).[30] Attaching a diethylene triamine-pentaacetic dianhydride (DTPAA) chelating moiety to either the six-membered ring diamino α-CD (Fig. 1a), or the seven-membered ring diamino β-CD (Fig. 1d), results in two different topologies of the studied Ln-CDs, as reflected from their schematic top views (Fig. 1b and e for Ln-α-CDs and Ln-β-CDs, respectively). Two series of Ln-CDs were selected for this study (Fig. 1c, f and S4–S9†) using the diamagnetic La^{3+} (*i.e.*, zero PCS induction) and three paramagnetic ions (Eu^{3+}, Ho^{3+} and Dy^{3+}) with increasing PCS induction capabilities.[49]

^{19}F-paraGEST experiments were performed with Ln-α-CD hosts and 4-(trifluoromethyl)benzylamine guest (**1**, Fig. 2a–e). With the diamagnetic La^{3+} ion, which has no PCS induction capability, no ^{19}F-paraGEST effect was observed (Fig. 2b for La-α-CD), probably because the $\Delta\omega > k_{ex}$ condition[42] is not met. Using a paramagnetic ion instead (Eu^{3+}, Ho^{3+} or Dy^{3+}, Fig. 2c–e), the PCS-induced $\Delta\omega$ might be sufficiently large to meet the prerequisites for GEST, as we previously demonstrated for Ln-α-CDs.[30] Note that the observed $\Delta\omega$ for each ^{19}F-paraGEST effect depends on the Ln^{3+} used and correlates with its Bleaney's constant.[50]

Indeed, as we demonstrated before for metallo-α-CDs, a clear ^{19}F-paraGEST effect was obtained for each studied paramagnetic Ln-α-CD with a specific $\Delta\omega$ between free and bound **1**. The $\Delta\omega$ values changed based on the PCS induction abilities of the Ln^{3+} from +0.8 ppm in Eu-α-CD (Fig. 2c) to −8.8 ppm in Ho-α-CD (Fig. 2d) and to −18.8 ppm in Dy-α-CD (Fig. 2e), as summarized in Table 1.

With Ln-β-CDs however (Fig. 2f–i), two ^{19}F-paraGEST effects were detected for the paramagnetic ions (marked as $\Delta\omega_1$ and $\Delta\omega_2$, Table 1), implying two different populations of bound guest complexes with two distinctive chemical shifts (*i.e.*, ω_1 and ω_2). While this phenomenon is small for Eu-β-CD (Fig. 2g), it becomes more pronounced with two sharp and spectrally resolved ^{19}F-paraGEST peaks for Ho-β-CD (Fig. 2h) and Dy-β-CD (Fig. 2i). Moreover, the separation between the two detected effects increases as the PCS induction increases (Fig. 2g–i, going from Eu^{3+} to Dy^{3+}). The chemical shift offset of the first effect, $\Delta\omega_1$, is similar to the observed in the corresponding Ln-α-CD, indicating a similar binding mode, which was previously demonstrated to involve the amine group of **1** facing the lanthanide center in Ln-α-CDs.[30] For example, $\Delta\omega_1 = -18.6$ ppm for **1** in Dy-β-CD (Fig. 2i) and $\Delta\omega_1 = -18.8$ ppm for **1** in Dy-α-CD (Fig. 2e). The same observation was obtained when comparing Eu-β-CD:**1** ($\Delta\omega_1 = 0.5$ ppm, Fig. 2g) to Eu-α-CD:**1** ($\Delta\omega_1 = 0.8$ ppm, Fig. 2c) and Ho-β-CD:**1** ($\Delta\omega_1 = -8.2$ ppm, Fig. 2h) to Ho-α-CD:**1** ($\Delta\omega_1 = -8.8$ ppm, Fig. 2d). Thus, we concluded that the second ^{19}F-paraGEST effect for each Ln-β-CD, which possesses a different $\Delta\omega$ value relative to the corresponding Ln-α-CD, implies on a different bound guest geometry of **1** with Ln-β-CDs.

To further elaborate on the source for this difference, the structures of the two Dy-CDs were modeled computationally (Fig. 3) using Grimme and coworkers' GFN2-xTB semiempirical method.[51] Dy-α-CD forms a round and bowl-like structure with a relatively small and confined interior (Fig. 3a–d) that limits the access of the guest to the lanthanide center. Meanwhile, Dy-β-CD, which is constructed with an extra sugar unit (Fig. 1d), possesses an elongated and bigger cavity (Fig. 3e–h) that may allow multiple binding modes. This could explain how only one species is observed by ^{19}F-paraGEST for the smaller Ln-α-CDs, while Ln-β-CDs, with their larger, asymmetric cavity, can host the guest in two (or more) ways. Note here that only the Dy^{3+} system was modelled and the other ions are expected to give similar results, as all the lanthanide ions tend to behave similarly. Similar observations were reported for computational modelling of related metallo-CDs.[39]

To test the nature of the observed ^{19}F-paraGEST phenomenon for Ln-β-CDs, three other fluorobenzylamine guests with different substitution patterns were considered and studied (**2–4**, Fig. 4). As previously shown for Dy-α-CD with the same

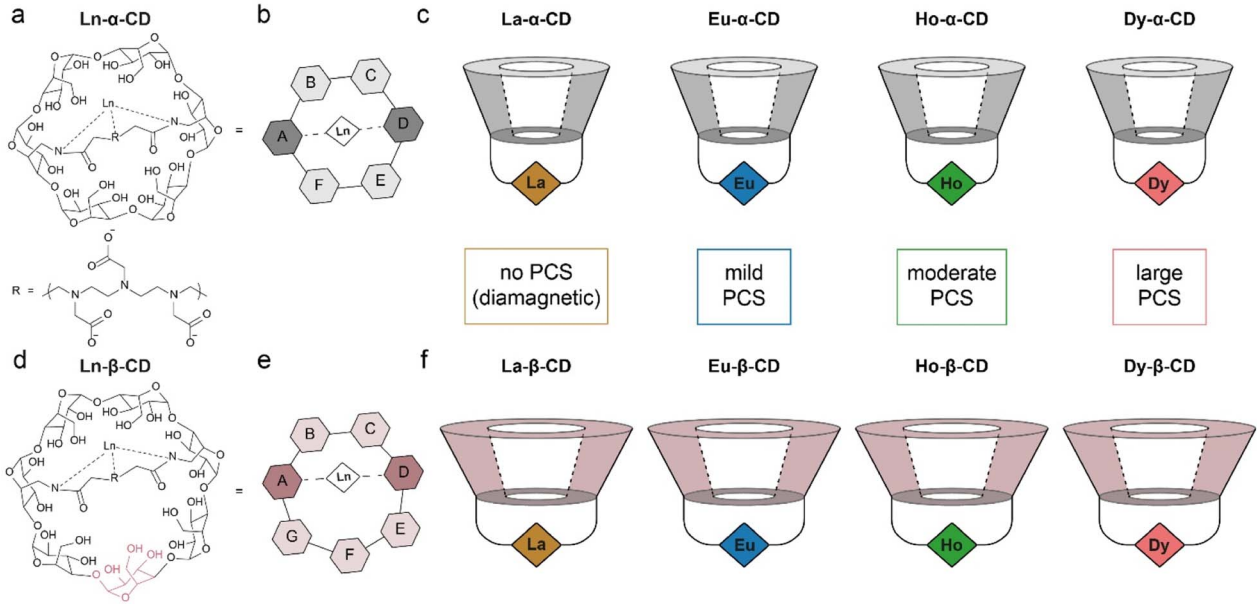

Fig. 1 The synthesized and studied families of Ln-CDs. (a) Molecular structure and (b) schematic representation of Ln-α-CD; (c) schematics of the previously synthesized Ln-α-CDs with their relative PCS capabilities (Ln^{3+} ions are represented as color diamonds); (d) molecular structure and (e) schematic representation of Ln-β-CD; (f) schematics of the Ln-β-CDs synthesized with their relative PCS capabilities (Ln^{3+} ions are represented as color diamonds). The data in panels a–c was adapted from ref. 30.

fluorinated guests,[30] only a single ^{19}F-paraGEST readout was observed for all three studied guests (Fig. 4b–d), similarly to the obtained with **1** (Fig. 2e). On the other hand, two ^{19}F-paraGEST peaks were observed for Dy-β-CD (Fig. 4e–g), in agreement with the obtained for guest **1** (Fig. 2i). Repeatedly, the $\Delta\omega_1$ values obtained for **2–4** with Dy-β-CD (Table S1†) are similar to the values obtained with Dy-α-CD, indicating a similar binding mode. Overall, these results show that for the different molecular guests examined (**1–4**, Fig. 2 and 4), when a paramagnetic Ln-α-CD was used as the metallo-CD

Table 1 The chemical shift offsets ($\Delta\omega$, ppm) of the ^{19}F-paraGEST effects for each studied host–guest system

Ln	Eu		Ho		Dy	
	$\Delta\omega_1$	$\Delta\omega_2$	$\Delta\omega_1$	$\Delta\omega_2$	$\Delta\omega_1$	$\Delta\omega_2$
Ln-α-CD:**1**	0.8	—	−8.8	—	−18.8	—
Ln-β-CD:**1**	0.5	−0.8	−8.2	−3.8	−18.6	−10.9

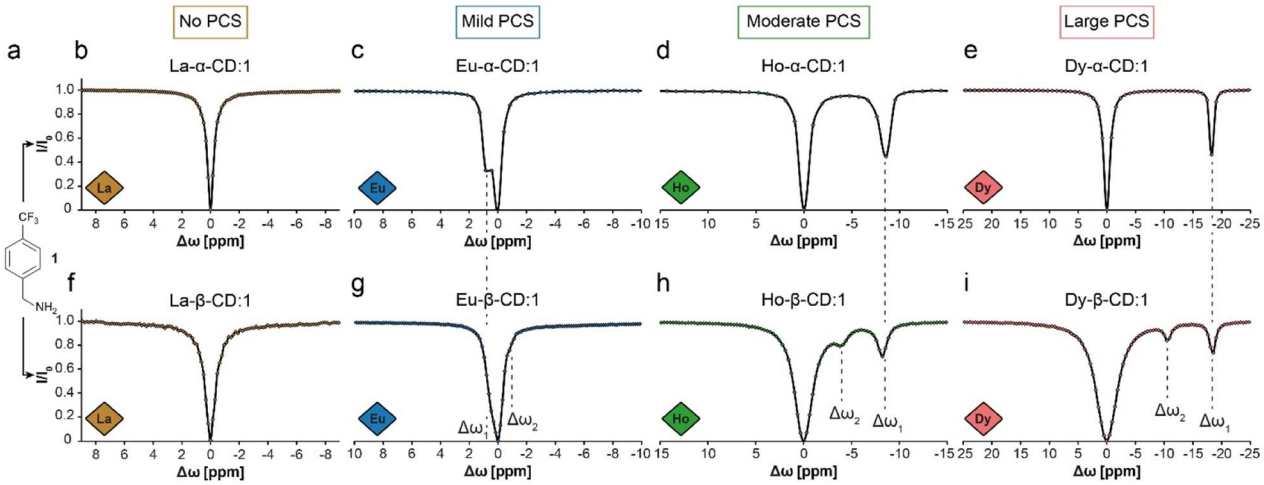

Fig. 2 ^{19}F-paraGEST z-spectra for solutions of **1** with different Ln-CDs. (a) The molecular structure of guest **1**. (b–e) The ^{19}F-paraGEST spectra obtained for **1** in the presence of different Ln-α-CD hosts. (f–i) The ^{19}F-paraGEST spectra obtained for **1** in the presence of different Ln-β-CD hosts. All experiments were performed at 25 °C with 1 : 100 host : guest solutions using an 11.7 T NMR spectrometer. The data in panels (b–e) was adapted from ref. 30.

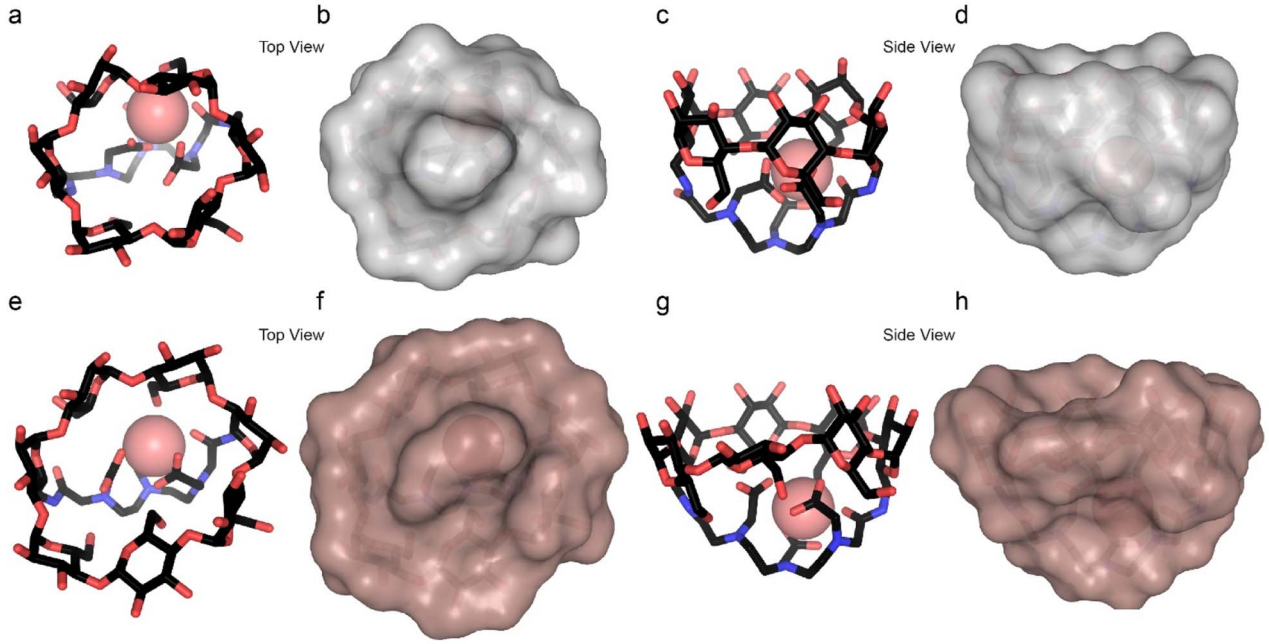

Fig. 3 Computational models. Top and side views of Dy-α-CD (a–d) and Dy-β-CD (e–h) showing both the molecular structure and the solvent exclude (Connolly) surface. Color scheme: C – black, O – red, N – blue, Dy – pink. Hydrogen atoms are omitted for clarity while Dy^{3+} is represented by a van der Waal radius sized sphere.

host, a single ^{19}F-paraGEST peak was obtained, and when a paramagnetic Ln-β-CD was used, two distinctive ^{19}F-paraGEST effects are clearly resolved.

There are three potential sources for the two ^{19}F-paraGEST signals obtained for complexes with Ln-β-CDs: (i) a 1 : 2 complex with two different bound guest geometries within

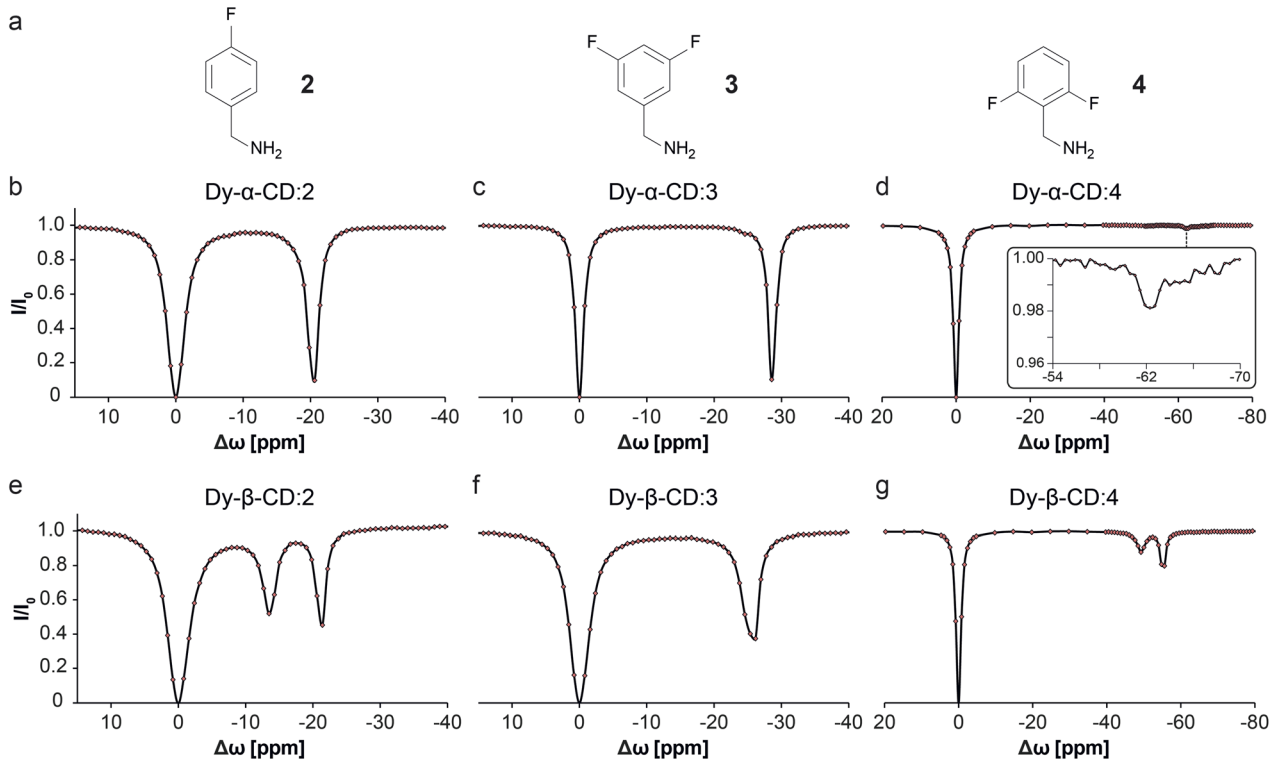

Fig. 4 ^{19}F-paraGEST z-spectra for solutions of Dy-α-CD or Dy-β-CD with different guest molecules. (a) The molecular structures of guests **2**, **3**, and **4**. (b–g) Z-spectra of the indicated host (as noted in each panel) and the corresponding guest. The data in panels b–d was adapted from ref. 30.

a single host molecule (Fig. 5a and S10a†), (ii) two 1 : 1 carceroisomers, where the guest is bound in a different orientation (Fig. 5b and S10b†), or (iii) a 2 : 2 complex of host dimer and two guest molecules in two orientations (Fig. 5c and S10c†). After confirming the complexation of **1** to La-β-CD using ^{1}H- and ^{19}F-NMR (Fig. 5d–f), we plotted a Job plot to determine the host : guest complex ratio, by measuring the UV-vis absorption for a series of solutions with different molar fractions of La-β-CD and **1** (Fig. S11 and Table S2†).[52,53] The Job's plot (Fig. 5g) shows a maximum at a molar fraction $R = 0.5$, which means that a 1 : 1 stoichiometry is observed. While this rules out option (i), the other two options (ii and iii) have 1 : 1 stoichiometries and could still explain the measurements. It should be pointed out that the Job's plot analysis might be limited in some cases, and other tools for analyzing UV-Vis absorption spectra can also be considered.[54]

Diffusion NMR is ideal for differentiating between monomeric, dimeric, or other multimeric assemblies of host : guest complexes in solutions.[55] A clear reduction in the diffusion coefficient of **1** (D_{guest}) was observed in the presence of the La-β-CD host (Fig. 5h and Tables S3, S4†), indicating the formation of a La-β-CD:**1** inclusion complex. On the other hand, the diffusion coefficient of La-β-CD (D_{host}) was not affected by the addition of guest **1**, eliminating the possibility of the formation of a dimeric 2 : 2 host : guest complex (option iii, Fig. 5c and S10c†). From the extracted D_{host} (0.255×10^{-5} cm^2 s^{-1}) and D_{guest} (0.682×10^{-5} cm^2 s^{-1}) values and the molecular weights of La-β-CD (M_{host} = 1626.2 g mol^{-1}) and **1** (M_{guest} = 75.15 g mol^{-1}), the

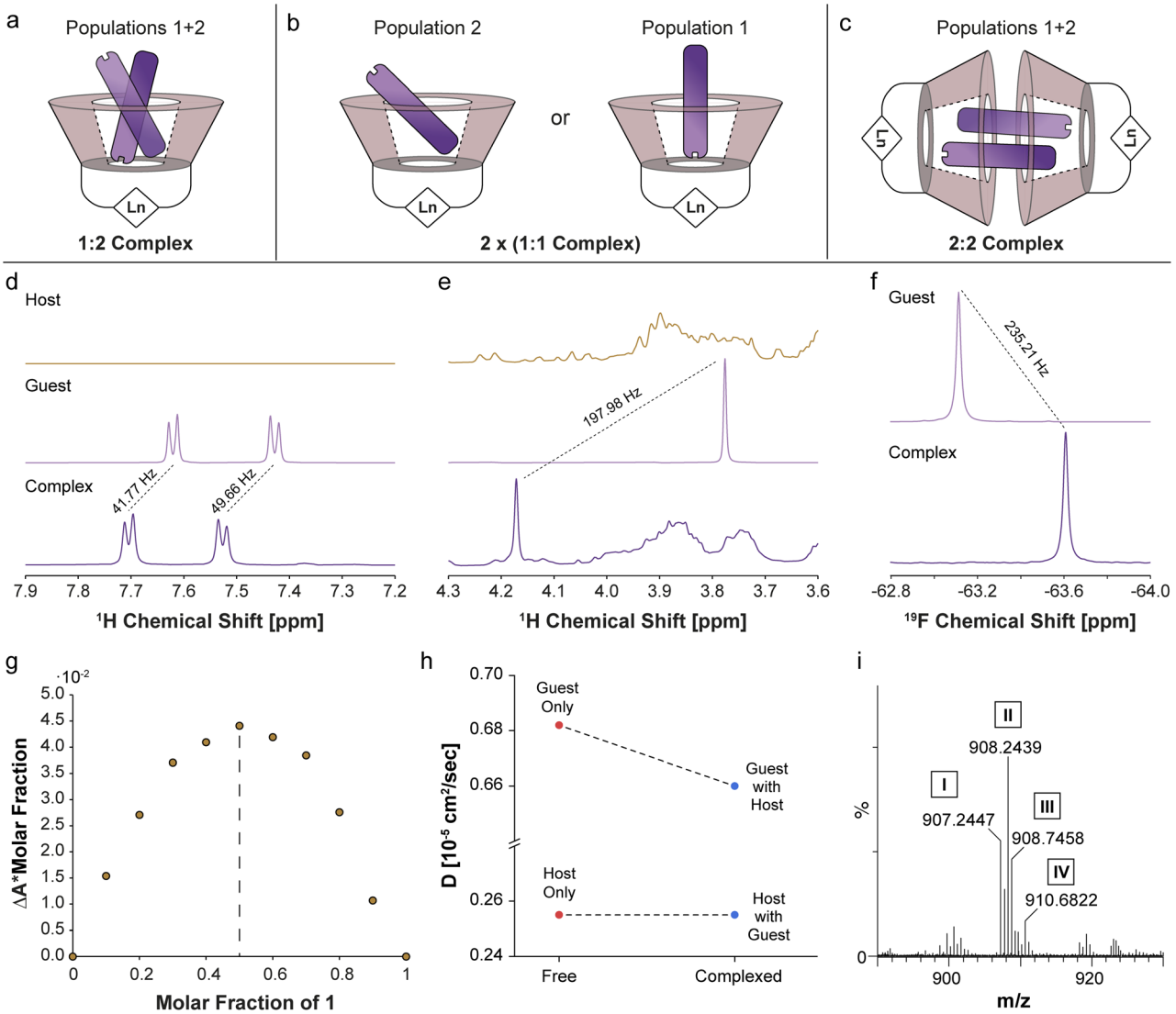

Fig. 5 Determination of Ln-β-CD:**1** complex stoichiometry. Schematic illustrations of the possible 1 : 2 (a), 1 : 1 (b) or 2 : 2 (c) stoichiometries for Ln-β-CD:**1** inclusion complexes. (d) The aromatic and (e) aliphatic regions of the ^{1}H-NMR spectrum of La-β-CD (brown), **1** (purple) and La-β-CD:**1** (dark purple). (f) ^{19}F-NMR spectra of **1** (purple) and La-β-CD:**1** (dark purple). (g) Job's plot describing the change in the UV absorbance (at 213 nm) of guest **1** as a function of the molar fraction. (h) Plot of the diffusion coefficients of La-β-CD and guest **1** (^{1}H-diffusion NMR) before and after complexation. (i) High-resolution electrospray ionization mass spectrometry of Eu-β-CD:**1** showing $[M_{1:1\ complex}]^{2+}$ (I), $[M_{1:1\ complex} + 2H]^{2+}$ (II), $[M_{1:1\ complex} + 3H]^{2+}$ (III), and $[M_{1:1\ complex} + 6H]^{2+}$ (IV).

host : guest stoichiometry[56] was found to be 1 : 1 in the La-β-CD:**1** complex, which means option ii (Fig. 5b and S10b†) describes the system. Additionally, this was confirmed by mass spectrometry (MS) analyses of Eu-β-CD:**1** (Fig. 5i and S12a†) and Dy-β-CD:**1** (Fig. S12b†), which indicated the formation of only 1 : 1 Ln-β-CD:**1** complexes with no evidence of other host : guest stoichiometries. Thus, three different methods, Job's plot (Fig. 5g), diffusion NMR (Fig. 5h), and MS (Fig. 5i), suggest the formation of two different 1 : 1 Ln-β-CD:**1** carceroisomers in solution (Fig. 5b and S10b†) as the source for the two ^{19}F-paraGEST effects (Fig. 2g–i and 4e–g), although these analytical tools are insensitive to the presence of two different types of such complexes (as revealed by ^{19}F-paraGEST).

From these results, we conclude that the geometries of the two Ln-β-CD:**1** populations involve two orientations or distances between the fluorine atoms of the guest and the Ln^{3+} ion in the host, resulting in a different Ln^{3+}-induced PCS effect for each orientation. In contrast, the smaller cavity of Ln-α-CD (Fig. 3a–d) allows only a single guest binding orientation. Using ^{19}F-paraGEST to measure the activation energy for guest dissociation ($E_{a,out}$, Fig. S13–S15†),[43] we found that more energy is needed to dissociate **1** from Dy-α-CD ($E_{a,out} = 66 \pm 3$ kJ mol^{-1}) than from Dy-β-CD ($E_{a,out} = 51 \pm 2$ and 44 ± 4 kJ mol^{-1} for $\Delta\omega_1$ and $\Delta\omega_2$, respectively). These observations imply the higher degrees of freedom possible for **1** in the larger and less symmetric cavity of Dy-β-CD (Fig. 3e–h), its weaker affinity to this seven-membered ring host (Fig. 1d and e), and support the ^{19}F-paraGEST results.

One of the strengths of ^{19}F-GEST is its ability to indirectly amplify NMR signals, allowing one to observe low-concentration host : guest complexes (relative to the dominant species in solution) and, as a result, to reveal otherwise unobservable species.[45] The detection level provided by ^{19}F-GEST depends on the guest's molar fraction (the ratio between complexed and free guest concentrations), amongst other factors such as k_{ex} or NMR relaxation properties. To determine if other undetected host–guest complexes exist at very low concentrations in solution, we increased the host : guest ratio to 1 : 10 (keeping the guest concentration constant) and compared the ^{19}F-paraGEST spectra for Dy-α-CD and Dy-β-CD (Fig. 6). No change in the number of ^{19}F-paraGEST peaks was observed for Dy-α-CD:**1** (single peak Fig. 6a), as measured for the 1 : 100 ratio (Fig. 2e). However, for Dy-β-CD:**1** an additional ^{19}F-paraGEST effect was observed at $\Delta\omega_3 = -29.3$ ppm (Fig. 6b), much further upfield than $\Delta\omega_1$ (−18.6 ppm) and $\Delta\omega_2$ (−10.9 ppm). This points out a third host–guest population coexisting in solution, which could be an additional orientation of **1** inside the larger, less symmetric cavity of Dy-β-CD (see Fig. S10† for some possible examples of guest inclusion possibilities). The characteristics of this additional population of Dy-β-CD:**1** complex should be further studied in the future (additional 1 : 1 host : guest complex or maybe a 1 : 2 one). These findings strengthen our conclusion of multiple coexisting Ln-β-CD:**1** complex populations in aqueous solutions – two major, but different, populations and at least one minor population. These findings may have implications when considering the applications of Ln-β-CD or Ln-α-CD in sensing and catalysis.

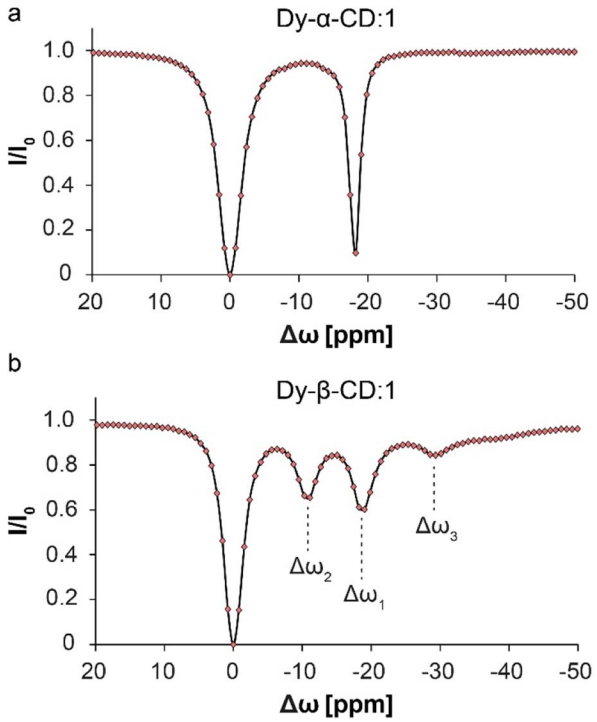

Fig. 6 ^{19}F-paraGEST z-spectra for solutions with high molar ratio of metallo-CD:**1**. (a) ^{19}F-paraGEST spectrum obtained for **1** with Dy-α-CD with a single peak for bound guest at $\Delta\omega_1 = -18.8$ ppm. The panel was adapted from ref. 30; (b) ^{19}F-paraGEST spectrum obtained for **1** with Dy-β-CD with three resolved peaks of bound guest at $\Delta\omega_1 = -18.6$ ppm, $\Delta\omega_2 = -10.9$ ppm, and $\Delta\omega_3 = -29.3$ ppm. Experiments were performed at 25 °C with solutions containing a 1 : 10 host : guest ratio on an 11.7 T NMR spectrometer.

Conclusions

We have synthesized two sets of metal-capped cyclodextrins – Ln-α-CDs and Ln-β-CDs – and experimentally demonstrated that the former lead to the formation of a single 1 : 1 host–guest complex in solution, while the latter form at least two different, coexisting 1 : 1 host–guest carceroisomers (Fig. 2, 4 and 6). Computational modelling showed that the two families of Ln-CD hosts differ in the size and shape of the cavity (Fig. 3), and the larger cavity of Ln-β-CD leads to possible multiple coordination modes of the guest to the lanthanide center. We showed that commonly used analytical tools, such as UV-vis spectroscopy, diffusion NMR, and mass spectrometry, cannot distinguish between the two types of Ln-β-CD : guest complexes (Fig. 5), which were only revealed by ^{19}F-paraGEST NMR. With this method, one can determine the k_{ex} values for the host-guest system, not attainable by other techniques, and detect very low concentrations of host–guest complexes. Using paramagnetic lanthanide ions with strong PCS capabilities (Ho^{3+} or Dy^{3+}) as substituents in Ln-CDs, the multiple populations of carceroisomers could be observed for different guest molecules. These findings could be important for future designs of metallo-cavitands as metallo-enzyme mimetics, which might require different degrees of freedom for a desired substrate. Since

paramagnetic CEST-MRI has been demonstrated for other paramagnetic metals, such as iron,[57] nickel,[58] and cobalt,[59] which are attractive targets for catalysis, we envision paraGEST could be a major breakthrough in the study of host–guest interactions in metal-capped molecular cavitands.

Data availability

The data that support the findings of this study are available upon a reasonable request from the corresponding author.

Author contributions

E. Goren and A. Bar-Shir. designed the study. E. Goren synthesized and purified all Ln-CDs. A. Falkovich performed all MS experiments, E. Goren and A. Falkovich analyzed the MS chromatograms. E. Goren and L. Avram performed all NMR experiments (1D NMR, GEST and Diffusion) and analyzed the data shown. E. Goren collected the UV-vis data, analyzed the data and plotted the Job's plot. Y. Diskin-Posner collected and analyzed preliminary crystal structure data that wasn't include in the paper. M. A. Iron performed computational calculations based on the data collected by Y. Diskin-Posner and configured the 3D structures. E. Goren and A. Bar-Shir wrote the manuscript.

Conflicts of interest

There are no conflicts to declare.

Acknowledgements

This work was supported by the Israel Science Foundation (ISF 1329/20), the Minerva Foundation, Helen and Martin Kimmel Institute for Magnetic Resonance Research, and Shimon and Golde Picker - Weizmann Annual Grant. Amnon Bar-Shir is the incumbent of the Helen and Milton A. Kimmelman Career Development Chair.

References

1 M. V. Rekharsky and Y. Inoue, *Chem. Rev.*, 1998, **98**, 1875–1918.
2 K. A. Connors, *Chem. Rev.*, 1997, **97**, 34.
3 A. Harada, *Acc. Chem. Res.*, 2001, **34**, 456–464.
4 Y.-M. Zhang, Y.-H. Liu and Y. Liu, *Adv. Mater.*, 2020, **32**, 1806158.
5 R. Breslow and S. D. Dong, *Chem. Rev.*, 1998, **98**, 1997–2012.
6 J. Szejtli, *Chem. Rev.*, 1998, **98**, 1743–1754.
7 C. J. Easton and S. F. Lincoln, *Chem. Soc. Rev.*, 1996, **25**, 163–170.
8 P. Jansook, N. Ogawa and T. Loftsson, *Int. J. Pharm.*, 2018, **535**, 272–284.
9 L. Tan, K.-G. Zhou, Y.-H. Zhang, H.-X. Wang, X.-D. Wang, Y.-F. Guo and H.-L. Zhang, *Electrochem. Commun.*, 2010, **12**, 557–560.
10 Q. Huang, L. Jiang, W. Liang, J. Gui, D. Xu, W. Wu, Y. Nakai, M. Nishijima, G. Fukuhara, T. Mori, Y. Inoue and C. Yang, *J. Org. Chem.*, 2016, **81**, 3430–3434.
11 M. Ceborska, K. Szwed, M. Asztemborska, M. Wszelaka-Rylik, E. Kicińska and K. Suwińska, *Chem. Phys. Lett.*, 2015, **641**, 44–50.
12 Y. Xiao, T. T. Tan and S. C. Ng, *Analyst*, 2011, **136**, 1433–1439.
13 X. Ma and H. Tian, *Acc. Chem. Res.*, 2014, **47**, 1971–1981.
14 L. Stricker, E. C. Fritz, M. Peterlechner, N. L. Doltsinis and B. J. Ravoo, *J. Am. Chem. Soc.*, 2016, **138**, 4547–4554.
15 M. Nakahata, Y. Takashima, H. Yamaguchi and A. Harada, *Nat. Commun.*, 2011, **2**, 511.
16 R. Breslow, G. Trainor and A. Ueno, *J. Am. Chem. Soc.*, 1983, **105**, 2739–2744.
17 R. Breslow and S. Chung, *Tetrahedron Lett.*, 1990, **31**, 631–634.
18 I. Tabushi, *Acc. Chem. Res.*, 1982, **15**, 66–72.
19 R. Breslow and L. E. Overman, *J. Am. Chem. Soc.*, 1970, **92**, 1075–1077.
20 B. Zhang and R. Breslow, *J. Am. Chem. Soc.*, 1997, **119**, 1676–1681.
21 D. Armspach and D. Matt, *Chem. Commun.*, 1999, 1073–1074, DOI: **10.1039/A902879J**.
22 R. Gramage-Doria, D. Armspach and D. Matt, *Coord. Chem. Rev.*, 2013, **257**, 776–816.
23 F. Ortega-Caballero, C. Rousseau, B. Christensen, T. E. Petersen and M. Bols, *J. Am. Chem. Soc.*, 2005, **127**, 3238–3239.
24 S. Guieu, E. Zaborova, Y. Blériot, G. Poli, A. Jutand, D. Madec, G. Prestat and M. Sollogoub, *Angew. Chem., Int. Ed.*, 2010, **49**, 2314–2318.
25 M. Jouffroy, R. Gramage-Doria, D. Armspach, D. Sémeril, W. Oberhauser, D. Matt and L. Toupet, *Angew. Chem., Int. Ed.*, 2014, **53**, 3937–3940.
26 B. Wang and M. Bols, *Chem.Eur. J.*, 2017, **23**, 13766–13775.
27 J. Meijide Suárez, O. Bistri-Aslanoff, S. Roland and M. Sollogoub, *ChemCatChem*, 2022, **14**, e202101411.
28 M. A. Mortellaro and D. G. Nocera, *J. Am. Chem. Soc.*, 1996, **118**, 7414–7415.
29 C. M. Rudzinski, D. S. Engebretson, W. K. Hartmann and D. G. Nocera, *J. Phys. Chem. A*, 1998, **102**, 7442–7446.
30 E. Goren, L. Avram and A. Bar-Shir, *Nat. Commun.*, 2021, **12**, 3072.
31 A. Grandeury, S. Petit, G. Gouhier, V. Agasse and G. Coquerel, *Tetrahedron: Asymmetry*, 2003, **14**, 2143–2152.
32 J. Tomeček, A. Čablová, A. Hromádková, J. Novotný, R. Marek, I. Durník, P. Kulhánek, Z. Prucková, M. Rouchal, L. Dastychová and R. Vícha, *J. Org. Chem.*, 2021, **86**, 4483–4496.
33 R. Rutenberg, G. Leitus, E. Fallik and E. Poverenov, *Chem. Commun.*, 2016, **52**, 2565–2568.
34 P. Timmerman, W. Verboom, F. C. J. M. van Veggel, J. P. M. van Duynhoven and D. N. Reinhoudt, *Angew. Chem., Int. Ed.*, 1994, **33**, 2345–2348.
35 C. Ihm, E. Jo, J. Kim and K. Paek, *Angew. Chem., Int. Ed.*, 2006, **45**, 2056–2059.
36 P. Mura, *J. Pharm. Biomed. Anal.*, 2014, **101**, 238–250.

37 P. Thordarson, *Chem. Soc. Rev.*, 2011, **40**, 1305–1323.
38 M. Guitet, P. Zhang, F. Marcelo, C. Tugny, J. Jiménez-Barbero, O. Buriez, C. Amatore, V. Mouriès-Mansuy, J.-P. Goddard, L. Fensterbank, Y. Zhang, S. Roland, M. Ménand and M. Sollogoub, *Angew. Chem., Int. Ed.*, 2013, **52**, 7213–7218.
39 P. Zhang, C. Tugny, J. Meijide Suárez, M. Guitet, E. Derat, N. Vanthuyne, Y. Zhang, O. Bistri, V. Mouriès-Mansuy, M. Ménand, S. Roland, L. Fensterbank and M. Sollogoub, *Chem*, 2017, **3**, 174–191.
40 K. M. Ward, A. H. Aletras and R. S. Balaban, *J. Magn. Reson.*, 2000, **143**, 79–87.
41 A. Bar-Shir, J. W. M. Bulte and A. A. Gilad, *ACS Chem. Biol.*, 2015, **10**, 1160–1170.
42 L. Avram and A. Bar-Shir, *Org. Chem. Front.*, 2019, **6**, 1503–1512.
43 R. Shusterman-Krush, L. Grimm, L. Avram, F. Biedermann and A. Bar-Shir, *Chem. Sci.*, 2021, **12**, 865–871.
44 L. Avram, M. A. Iron and A. Bar-Shir, *Chem. Sci.*, 2016, **7**, 6905–6909.
45 L. Avram, V. Havel, R. Shusterman-Krush, M. A. Iron, M. Zaiss, V. Šindelář and A. Bar-Shir, *Chem.Eur. J.*, 2019, **25**, 1687–1690.
46 L. Avram, A. D. Wishard, B. C. Gibb and A. Bar-Shir, *Angew. Chem., Int. Ed.*, 2017, **56**, 15314–15318.
47 I. Horin, S. Slovak and Y. Cohen, *Chem.Eur. J.*, 2023, e202301628.
48 J. Wang, L. Avram, Y. Diskin-Posner, M. J. Bialek, W. Stawski, M. Feller and R. Klajn, *J. Am. Chem. Soc.*, 2022, **144**, 21244–21254.
49 Z. K. Subha Viswanathan, K. N. Green, S. James Ratnakar and A. Dean Sherry, *Chem. Rev.*, 2010, **110**, 59.
50 O. A. Blackburn, R. M. Edkins, S. Faulkner, A. M. Kenwright, D. Parker, N. J. Rogers and S. Shuvaev, *Dalton Trans.*, 2016, **45**, 6782–6800.
51 C. Bannwarth, S. Ehlert and S. Grimme, *J. Chem. Theory Comput.*, 2019, **15**, 1652–1671.
52 B. Rajbanshi, S. Saha, K. Das, B. K. Barman, S. Sengupta, A. Bhattacharjee and M. N. Roy, *Sci. Rep.*, 2018, **8**, 13031.
53 J. S. Renny, L. L. Tomasevich, E. H. Tallmadge and D. B. Collum, *Angew. Chem., Int. Ed.*, 2013, **52**, 11998–12013.
54 D. Brynn Hibbert and P. Thordarson, *Chem. Commun.*, 2016, **52**, 12792–12805.
55 Y. Cohen, L. Avram and L. Frish, *Angew. Chem., Int. Ed.*, 2005, **44**, 520–554.
56 A. R. Waldeck, P. W. Kuchel, A. J. Lennon and B. E. Chapman, *Prog. Nucl. Magn. Reson. Spectrosc.*, 1997, **30**, 39–68.
57 S. J. Dorazio, P. B. Tsitovich, K. E. Siters, J. A. Spernyak and J. R. Morrow, *J. Am. Chem. Soc.*, 2011, **133**, 14154–14156.
58 A. O. Olatunde, S. J. Dorazio, J. A. Spernyak and J. R. Morrow, *J. Am. Chem. Soc.*, 2012, **134**, 18503–18505.
59 S. J. Dorazio, A. O. Olatunde, J. A. Spernyak and J. R. Morrow, *Chem. Commun.*, 2013, **49**, 10025–10027.